Supporting Information

Toward high performance indacenodithiophene-based small-molecule organic solar cells: investigation of the effect of fused aromatic bridge on the device performance

Jin-Liang Wang,*[a][+] Fei Xiao,[a][+] Jun Yan,[b][+] Kai-Kai Liu,[a] Zheng-Feng Chang,[a] Ru-Bo Zhang,*[a] Hong-Bin Wu,*[b] and Yong Cao [b]

[a]Beijing Key Laboratory of Photoelectronic/Electrophotonic Conversion Materials, School of Chemistry, Beijing Institute of Technology, 5 South Zhongguancun Street, Beijing, 100081, China.
E-mail: jinlwang@bit.edu.cn
[b]Institute of Polymer Optoelectronic Materials and Devices, State Key Laboratory of Luminescent Materials and Devices, South China University of Technology, 381 Wushan Road, Guangzhou, 510640, China.
E-mail: hbwu@scut.edu.cn

[+] These authors contributed equally to this work.

1. Experimental Section

Characterization and measurement. The values of power conversion efficiency were determined from *J*-V characteristics measured by a Keithley 2400 source-measurement unit under AM 1.5G spectrum from a solar simulator (Oriel model 91192). Masks made from laser beam cutting technology with well-defined area of 16.0 mm^2 were attached to define the effective area for accurate measurement. Solar simulator illumination intensity was determined using a monocrystal silicon reference cell (Hamamatsu S1133, with KG-5 visible color filter) calibrated by the National Renewable Energy Laboratory (NREL). EQE values of the encapsulated devices were measured by using an integrated system (Enlitech, Taiwan, China) and a lock-in amplifier with a current preamplifier under short-circuit conditions. The devices were illuminated by monochromatic light from a 75 W xenon lamp. The light intensity was determined by using a calibrated silicon photodiode.

Transient photovoltage and transient photocurrent measurements: Transient photovoltage measurement was performed by holding the devices at open-circuit condition under illumination of a 100W tungsten halogen lamp. The devices were connected to an oscilloscope (Tektronix DPO4104, 1GHz) that has an input impedance of the oscilloscope of 1 MΩ to hold the device at open circuit. The excitation pulse was generated using a pulsed laser (OPOTEK Vibrant 355, with a 5 ns optical pulse). The perturbation light intensity was attenuated by a set of neutral density filter so that the amplitude of TPV is much less than Voc. Transient photocurrent measurement was performed with the device being held at short circuit condition by connecting the device to the ground through a small resistor. The

resulting current transient was measured using an oscilloscope (Tektronix DPO4104, 1GHz) in parallel with a small resistor of 50 Ω. The excitation pulse was generated using a pulsed laser (OPOTEK Vibrant 355, with a 5 ns optical pulse).

SCLC device fabrication and characterization: The structures of hole only and electron only device are ITO/PEDOT/donor materials: $PC_{71}BM/MoO_3/Al$ and ITO/ZnO/PFN/donor materials:$PC_{71}BM/Ca/Al$, respectively. The mobility was determined by fitting the dark current to the model of the filed-independent space charge limited current (SCLC) according to the Mott-Gurney law, given by

$J = \frac{9}{8}\varepsilon_0\varepsilon_r\mu_h\frac{V^2}{L^3}$ for hole only device and $J = \frac{9}{8}\varepsilon_0\varepsilon_r\mu_e\frac{V^2}{L^3}$ for electron only device

Where J is the current density, ε_0 is the permittivity of free space, ε_r is the relative permittivity of the material, μ_h is the hole mobility, μ_e is the hole mobility, L is the film thickness of the active layer, and V is the effective voltage which is determined by subtracting the built-in voltage (V_{bi}) from the applied voltage ($V = V_{appl} - V_{bi}$). V_{bi} was estimated to be 0.4 V based on the dark *J*-*V* curve of our hole-only device, at high voltages, the *J*-*V* characteristics of the devices can be consistently described by Mott-Gurney law, thus the hole and electron mobility can be directly calculated from *J*-V curves.

Theoretical analysis details. In the DFT calculations the side-chains on the IDT and terminal groups were replaced by methyl group to improve computational efficiency. The studied molecules should have several possible rotation isomers, whose significant close-to-planarity structures could be obtained through rotation of the bonds between the electron donor and acceptor in these five molecules. The two main conformations of each molecule thus show characterized by straight and zigzag conformation, respectively, and have been optimized in the gas phase at the level of B3LYP/6-31G(d). All calculations were performed with Gaussian 09 package.

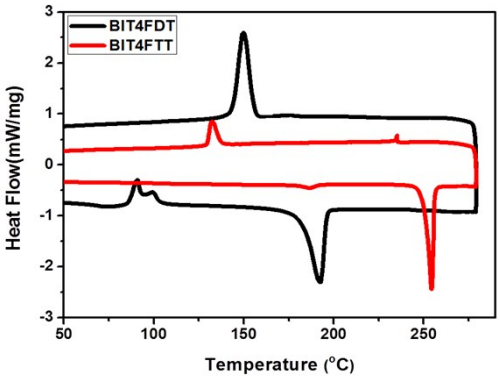

Figure S1. DSC traces of **BIT4FDT** and **BIT4FTT** with a heating/cooling circle under N_2 atmosphere.

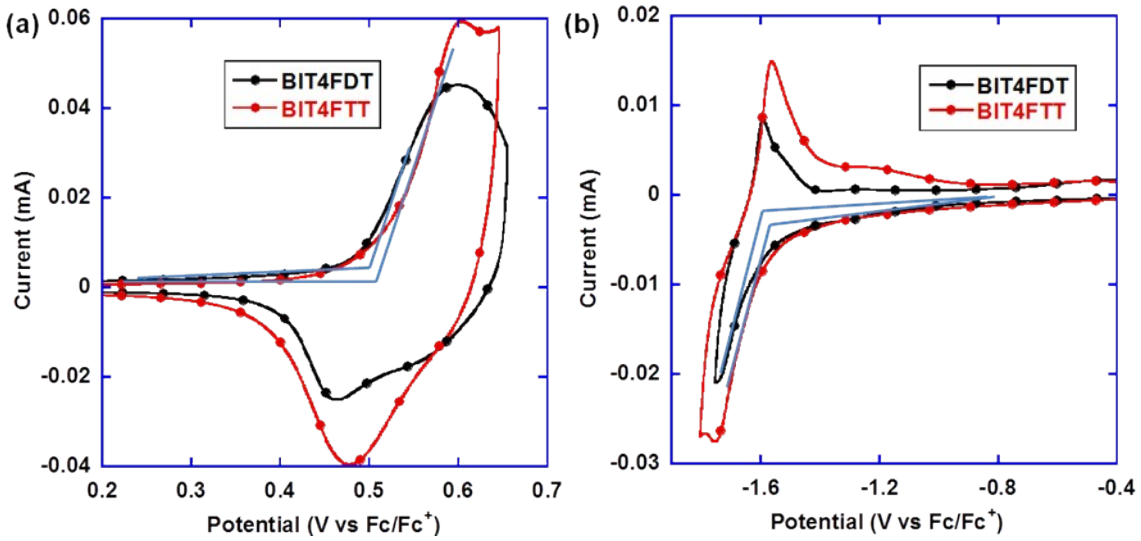

Figure S3.Cyclic voltammogram of **BIT4FDT** and **BIT4FTT** films on Pt electrode in 0.1 M Bu_4NPF_6 in CH_3CN solution versus $Ag/AgNO_3$ (0.01 M in anhydrous acetonitrile) reference electrode with a scan rate of 50 mV/s.

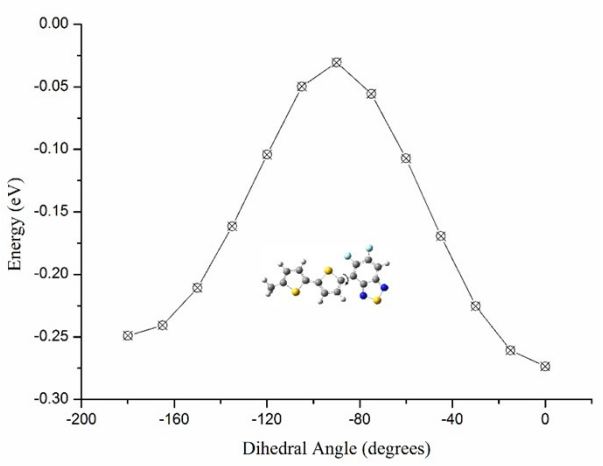

Figure S4. DFT derived potential energy for the torsional degree of freedom between 0 and 180 degrees for the terminal group (similar with compound **1**) of our small molecules (The lowest energy molecular configuration is shown in figure).

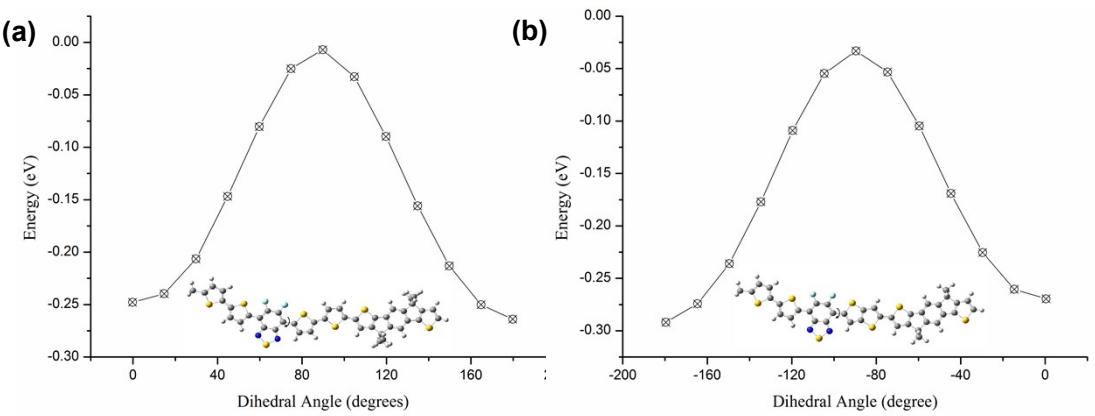

Figure S5. DFT derived potential energy for the torsional degree of freedom between 0 and 180 degrees for directions of the inner thiophene rings next to the BT unit of **BIT4FDT** (a) and **BIT4FTT** (b) (The lowest energy molecular configuration are shown in figures).

Table S1. Summary of calculated parameters for these small molecules using DFT B3LYP/6-31G(d) method.[a]

Compd	HOMO (eV)	LUMO (eV)	ΔE_g (eV)	f	M_{01} (D)
BIT4FDT	-4.68	-2.82	1.86	4.6	9.1
BIT4FTT	-4.68	-2.83	1.85	4.4	8.9

[a]f: oscillator strength; M_{01}: transition dipole moment.

Table S2. A summary of the device performances of the organic solar cells from blend films of these small-molecules and **$PC_{71}BM$** after $CHCl_3$ or THF vapor annealing.

Active layer	J_{sc} (mA/cm^2)	V_{oc} (V)	FF	PCE (%)
BIT4FDT/$PC_{71}BM$ (1:3) [a]	3.40	0.50	0.59	1.00
BIT4FDT/$PC_{71}BM$ (1:3) [b]	6.22	0.65	0.62	2.53
BIT4FTT/$PC_{71}BM$ (1:3) [a]	8.32	0.72	0.68	4.05
BIT4FTT/$PC_{71}BM$ (1:3) [b]	9.23	0.76	0.72	5.07

[a]treatment with $CHCl_3$ vapor annealing for 30 s. [b]treatment with THF vapor annealing for 60 s.

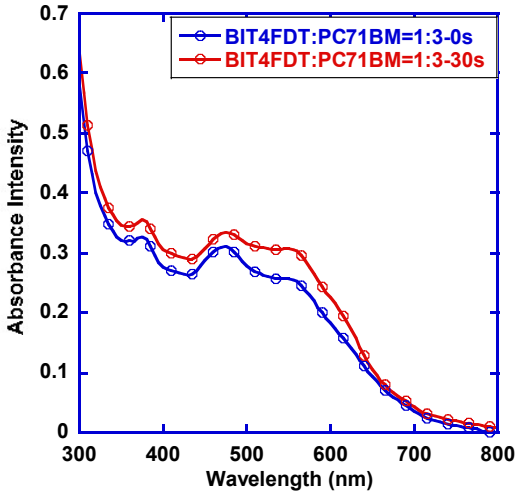

Figure S6. Absorption spectra of **BIT4FDT:** $PC_{71}BM$ blend films before/after treatment with CH_2Cl_2 vapor annealing.

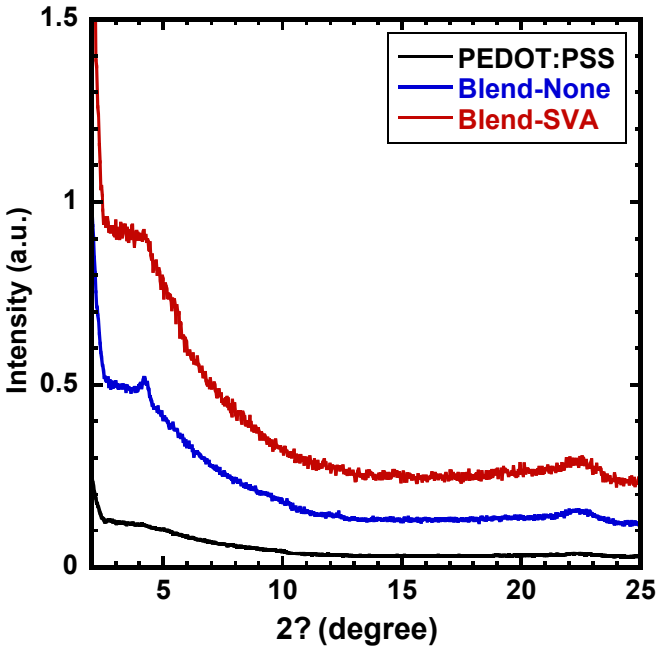

Figure S7. XRD patterns of **BIT4FTT**/$PC_{71}BM$ blend films before/after treatment with CH_2Cl_2 vapor annealing.

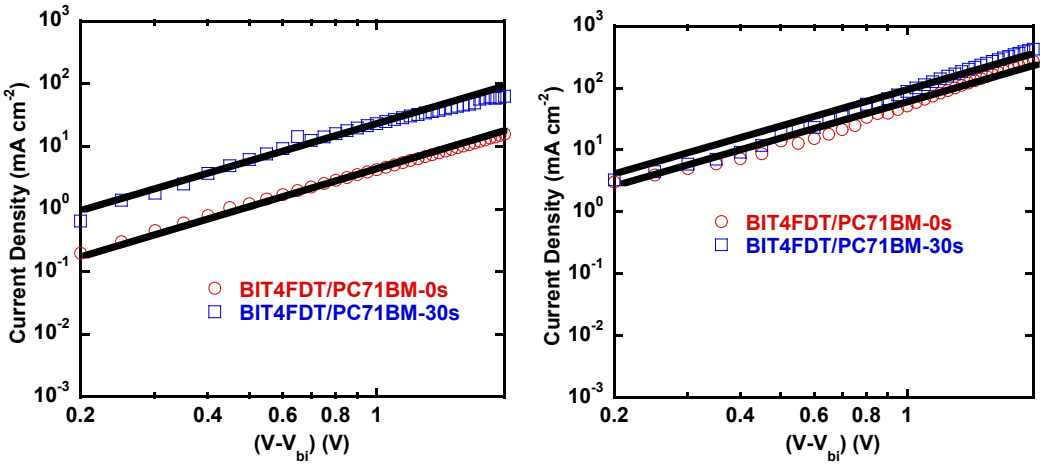

Figure S8.The *J-V* plots of the devices with (a) a configuration of ITO/PEDOT/ **BIT4FDT**:$PC_{71}BM$/Au for hole only device and (b) a configuration of ITO/ZnO/PFN/**BIT4FDT**:$PC_{71}BM$/Ca/Al for electron only device. The open circles and squares are for the device before and after CH_2Cl_2 vapor annealing for 30 s, respectively. The solid lines represent the best fitting from the space-charge-limited-current model.

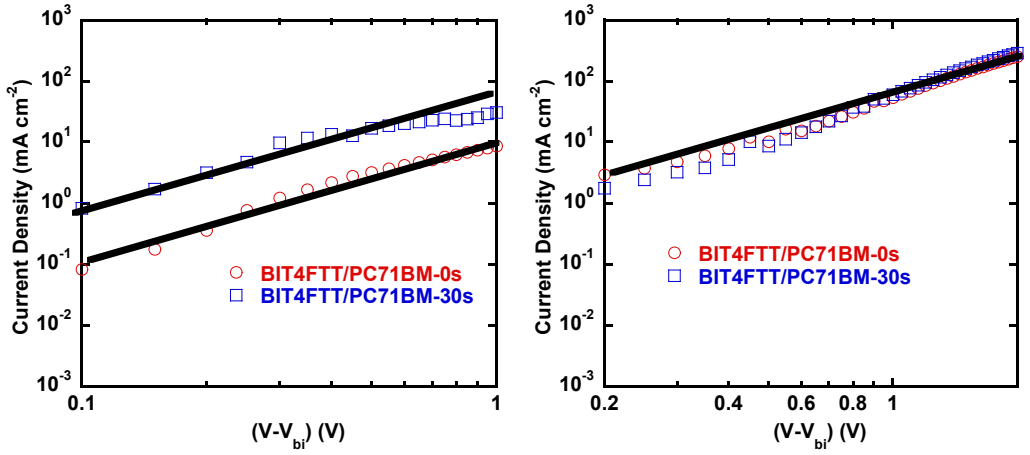

Figure S9: The *J-V* plots of the devices with (a) a configuration of ITO/PEDOT/ **BIT4FTT**:$PC_{71}BM$/Au for hole only device and (b) a configuration of ITO/ZnO/PFN/**BIT4FTT**:$PC_{71}BM$/Ca/Al for electron only device. The open circles and squares are for the device before and after CH_2Cl_2 vapor annealing for 30 s, respectively. The solid lines represent the best fitting from the space-charge-limited-current model.

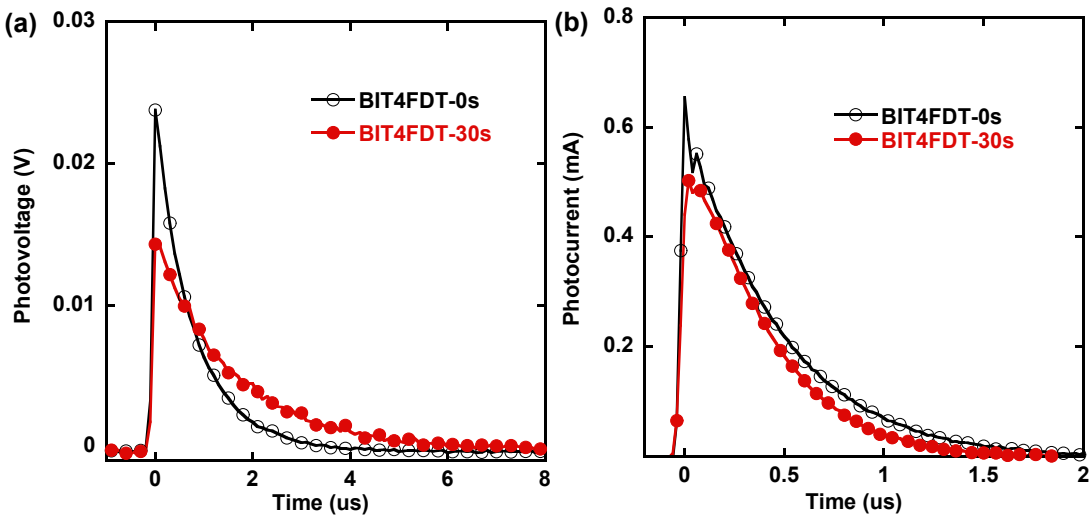

Figure S10: (a) Transient photovoltage and (b) Transient photocurrent signals for **BIT4FDT/PC$_{71}$BM** devices before and after CH_2Cl_2 vapor annealing, measured under 1sun illumination and open-circuit voltage conditions using the same intensity laser pulse.

2. Copies of ^{1}H and ^{13}C NMR Spectra

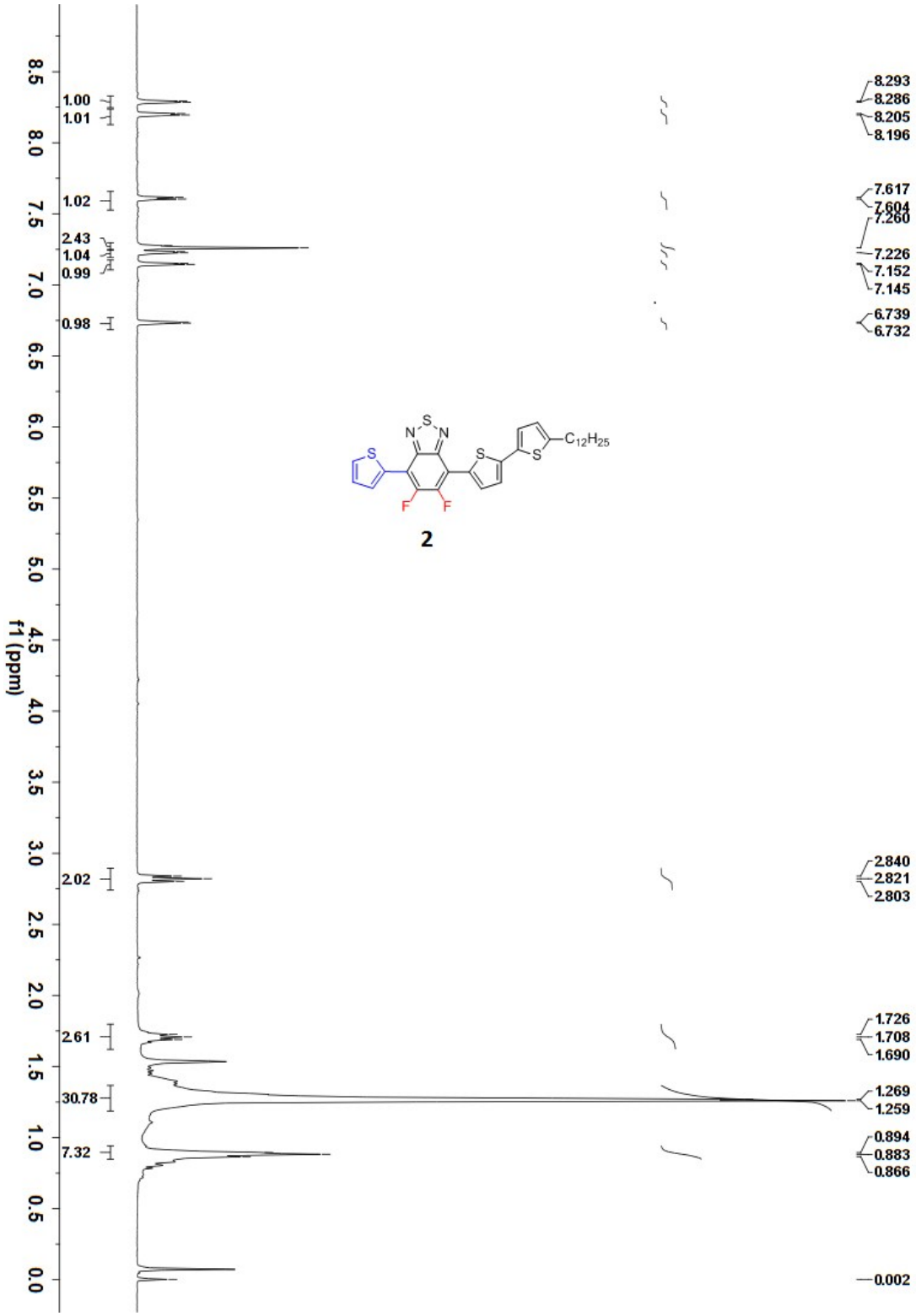

^{1}H NMR spectrum for compound **2**

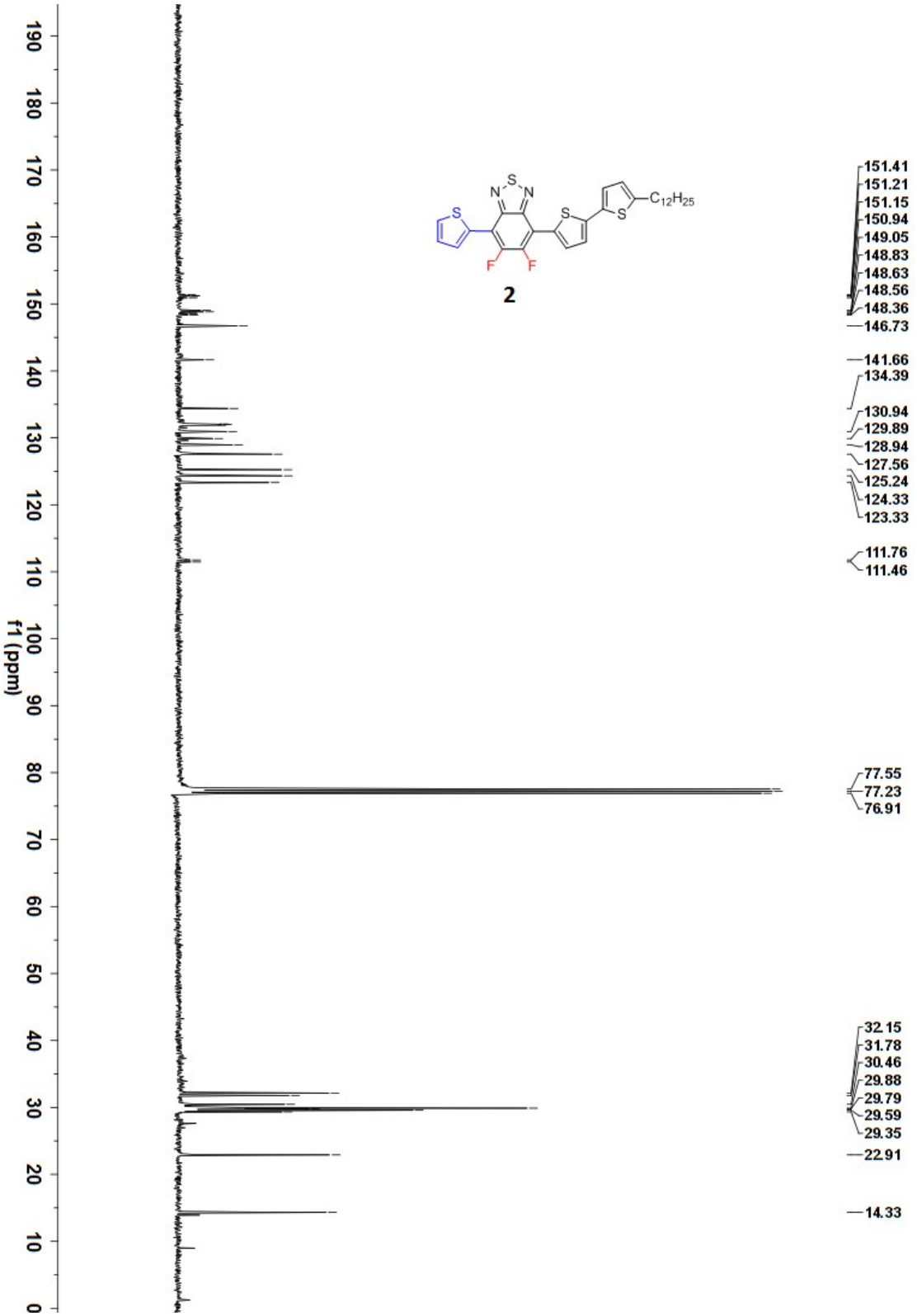

^{13}C NMR spectrum for compound **2.**

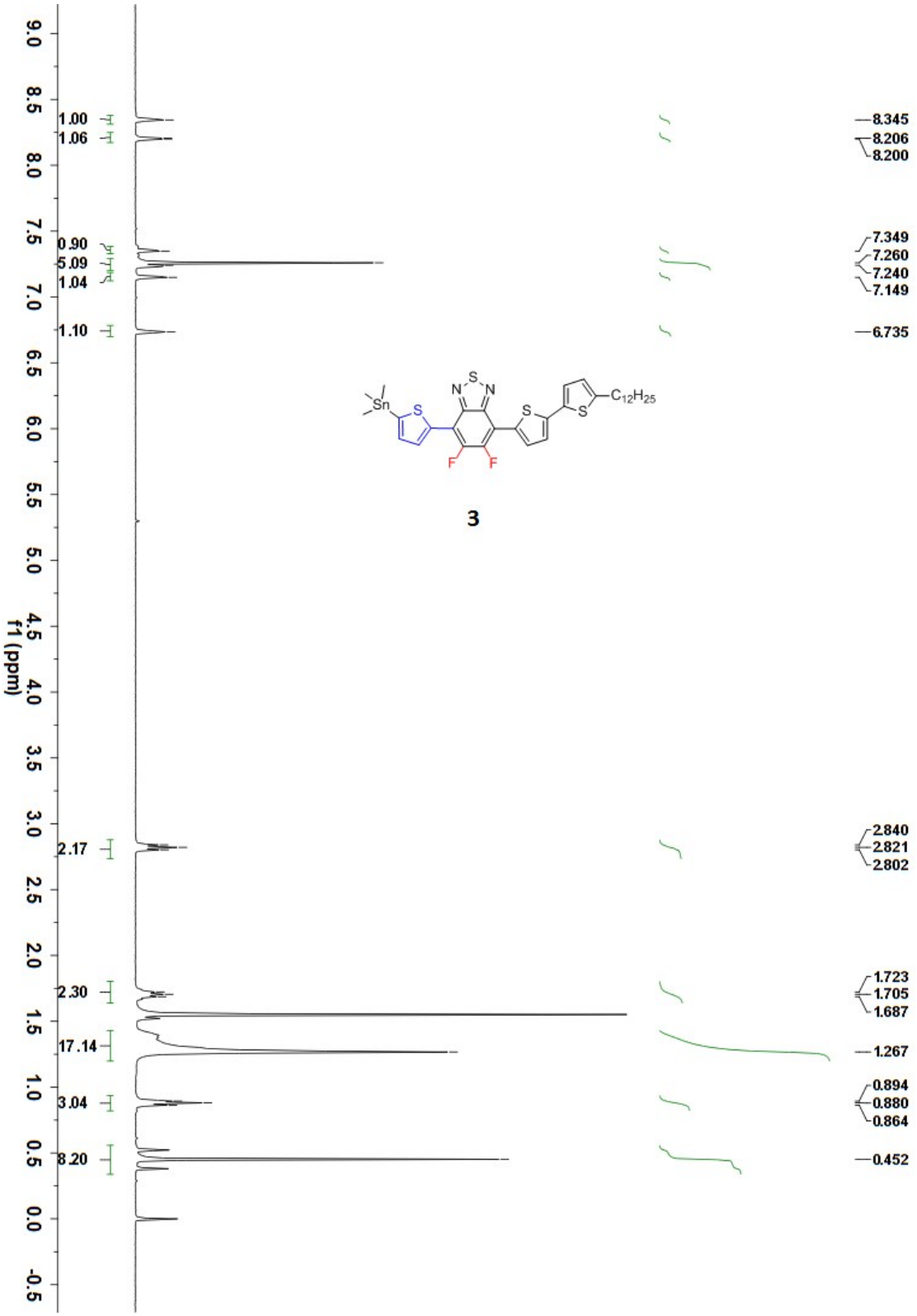

3

[1]H NMR spectrum for compound **3**

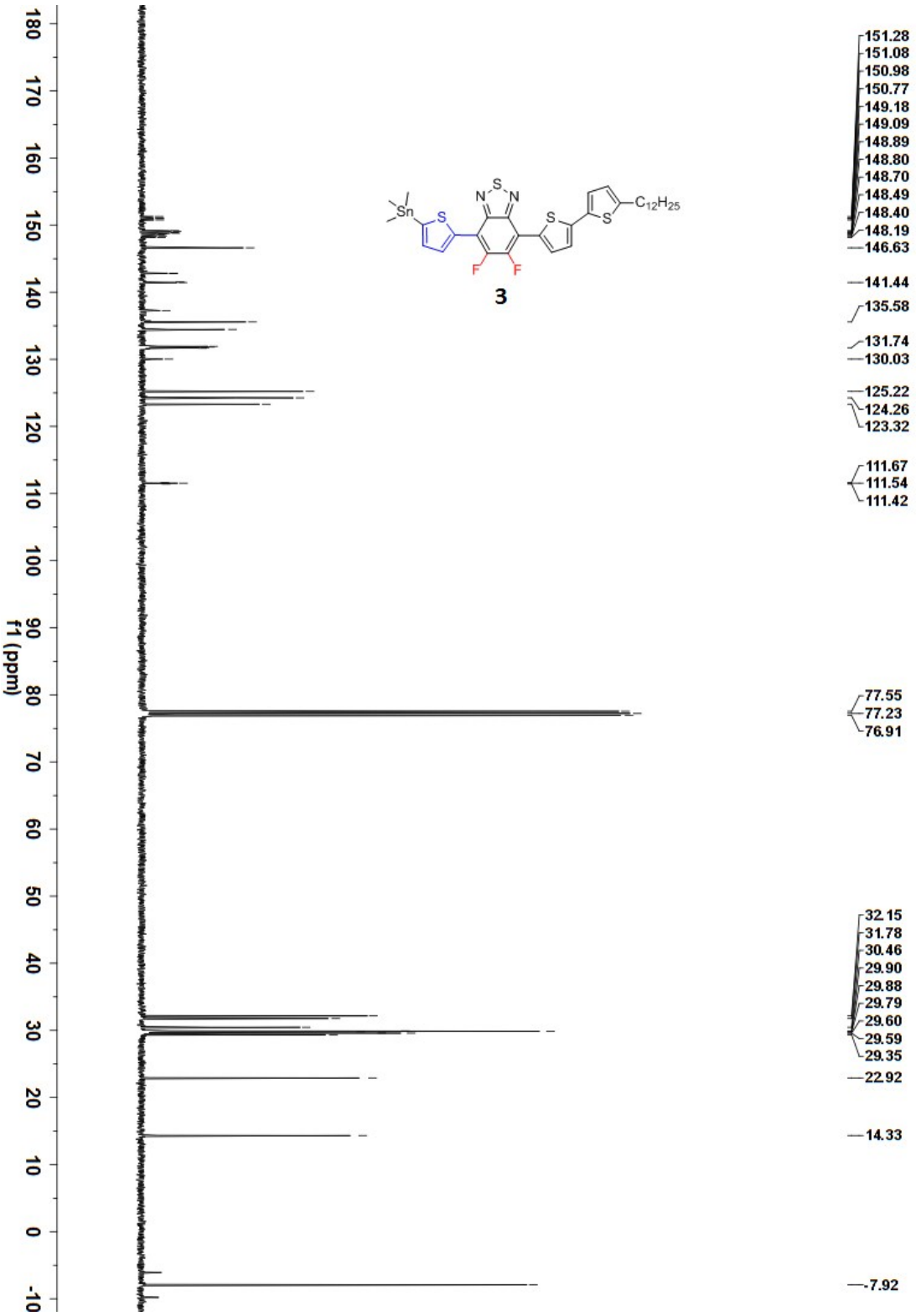

^{13}C NMR spectrum for compound **3.**

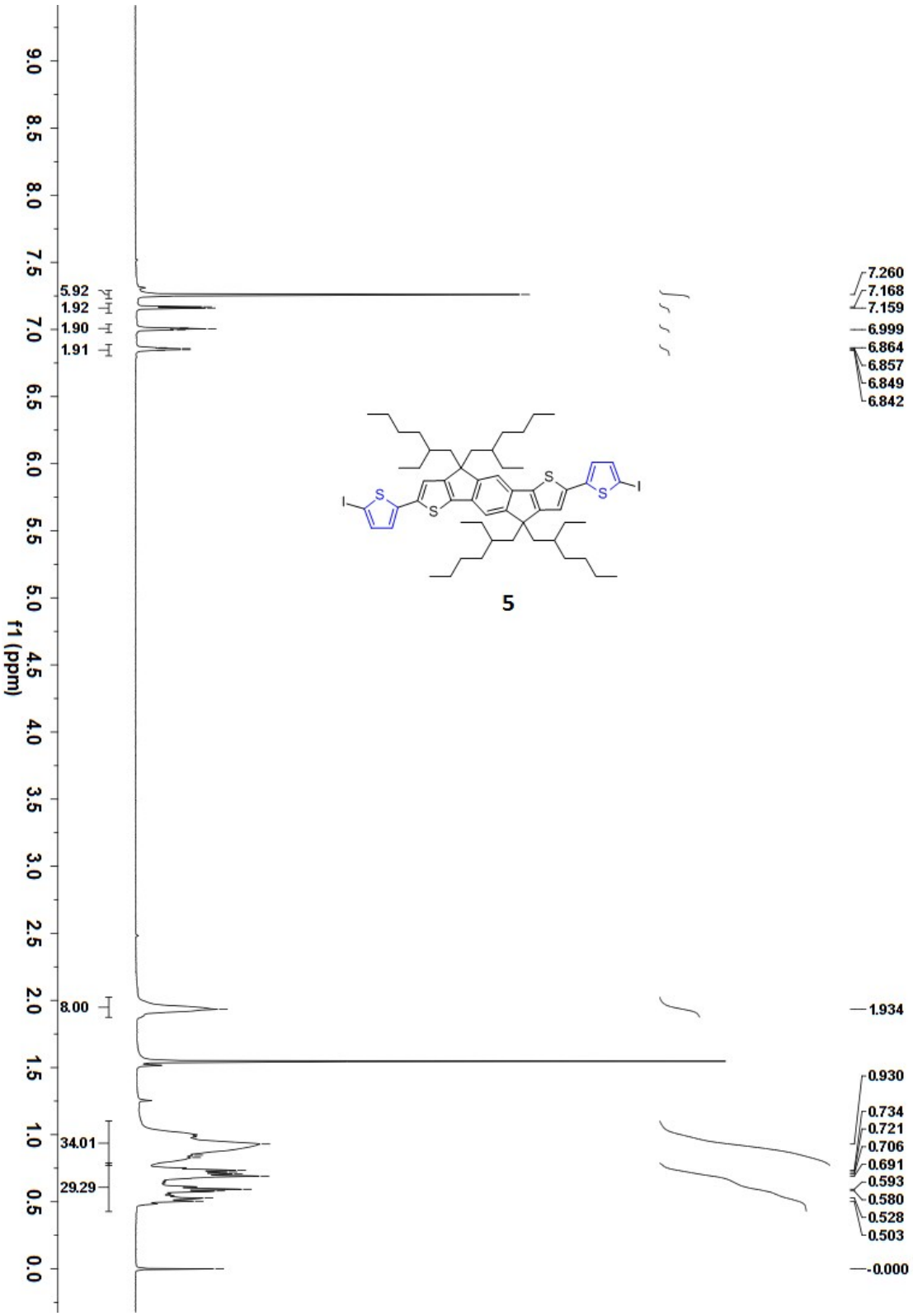

^{1}H NMR spectrum for compound **5**

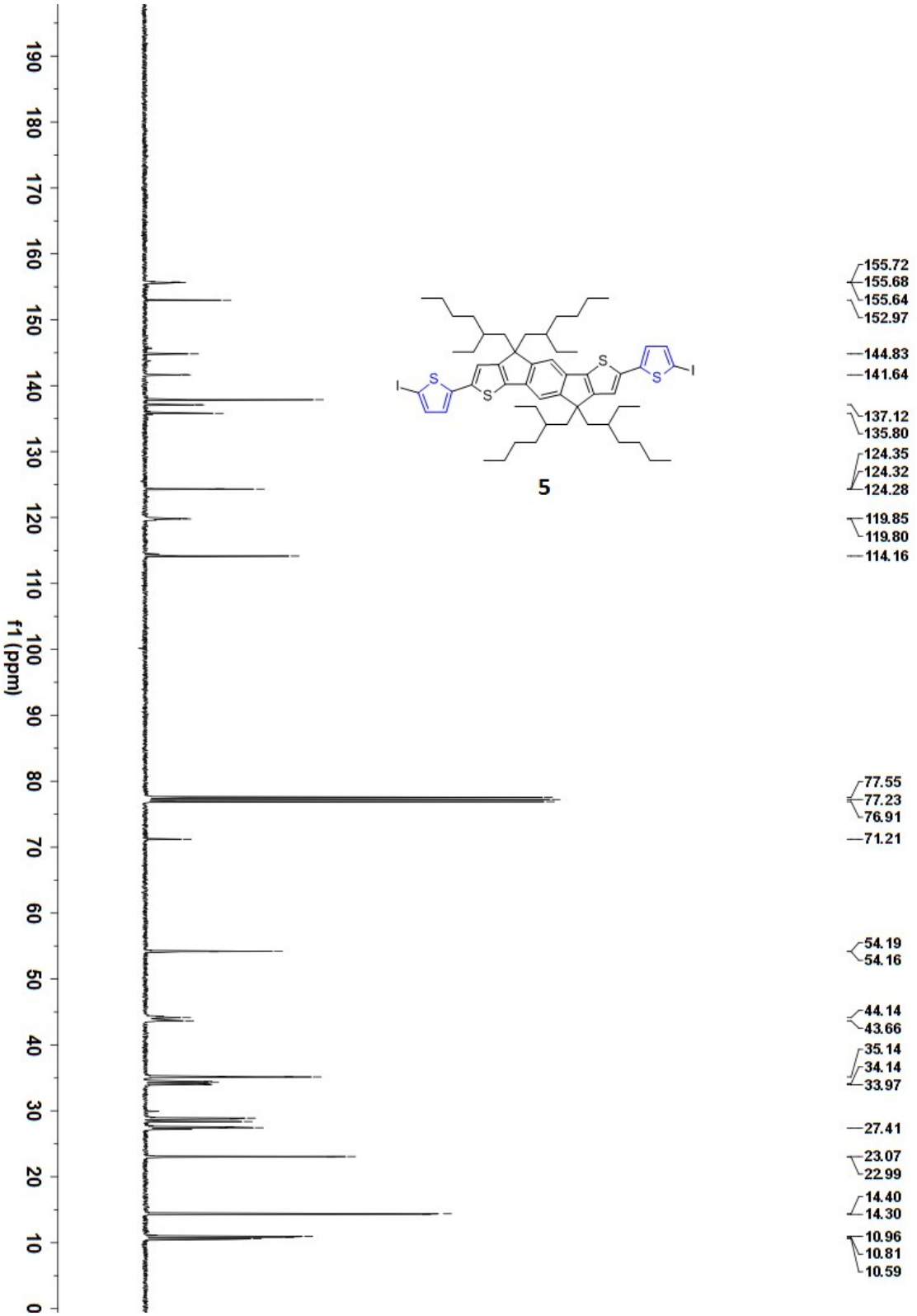

^{13}C NMR spectrum for compound **5**

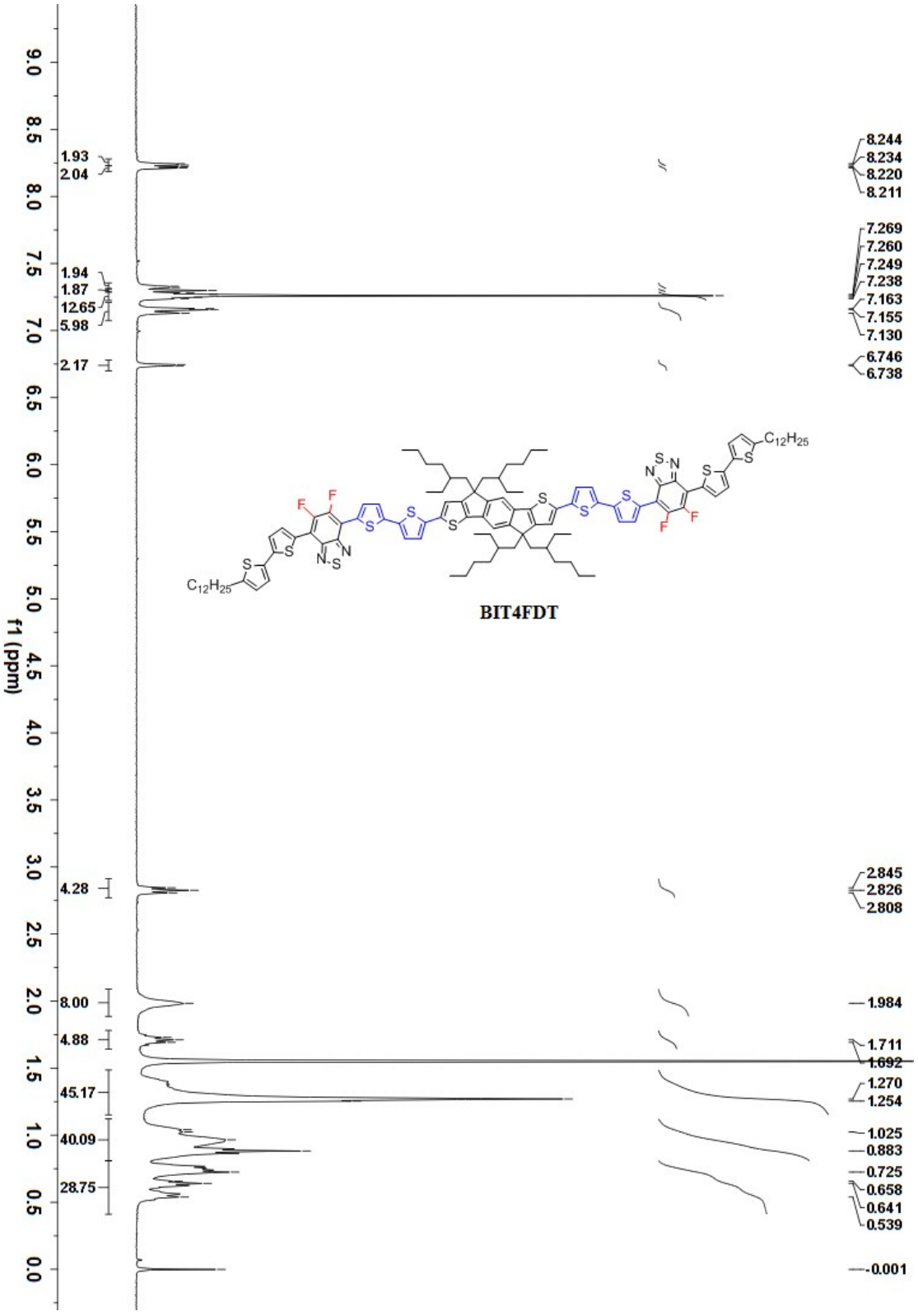

^{1}H NMR spectrum for **BIT4FDT**

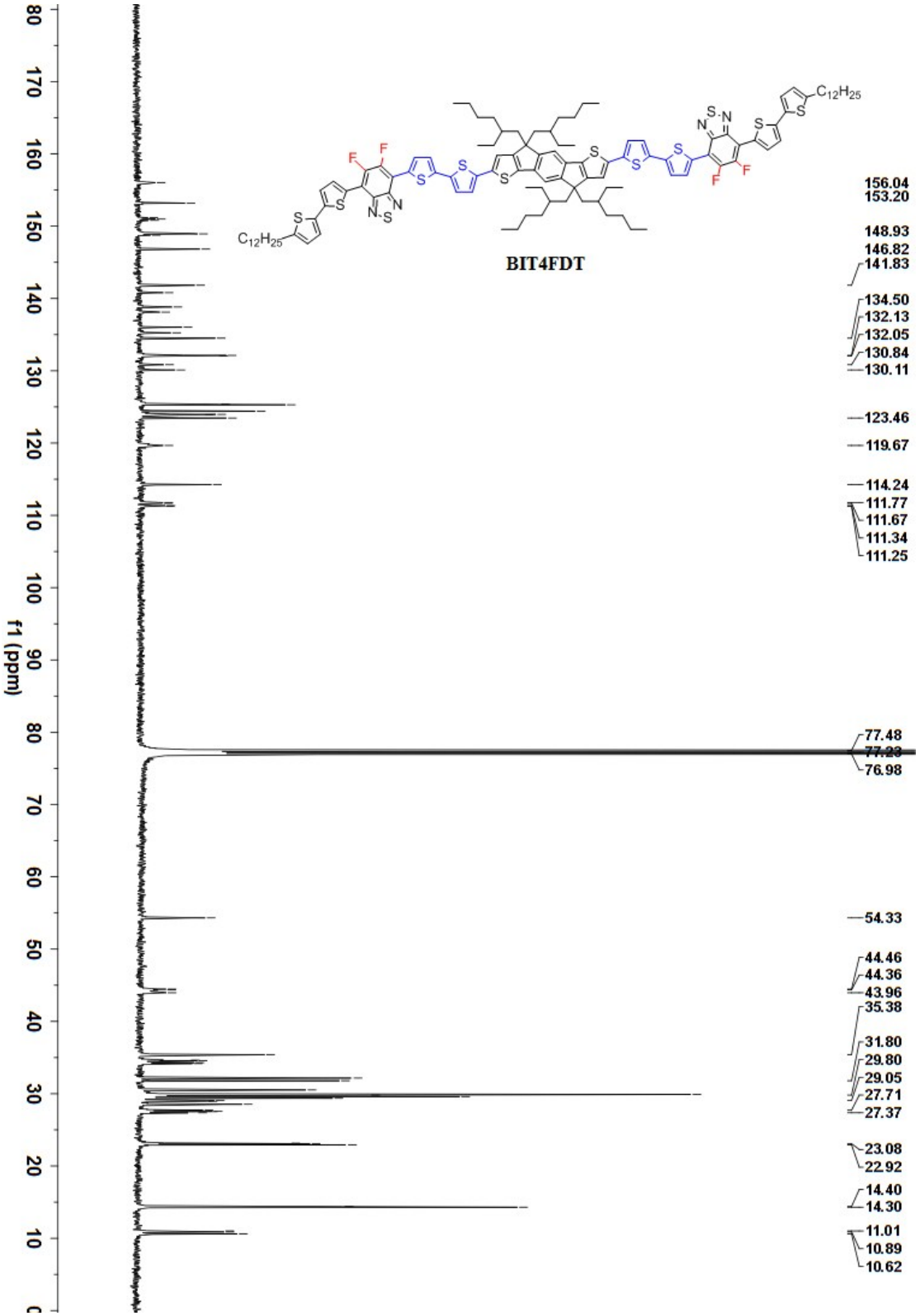

^{13}C NMR spectrum for compound **BIT4FDT**

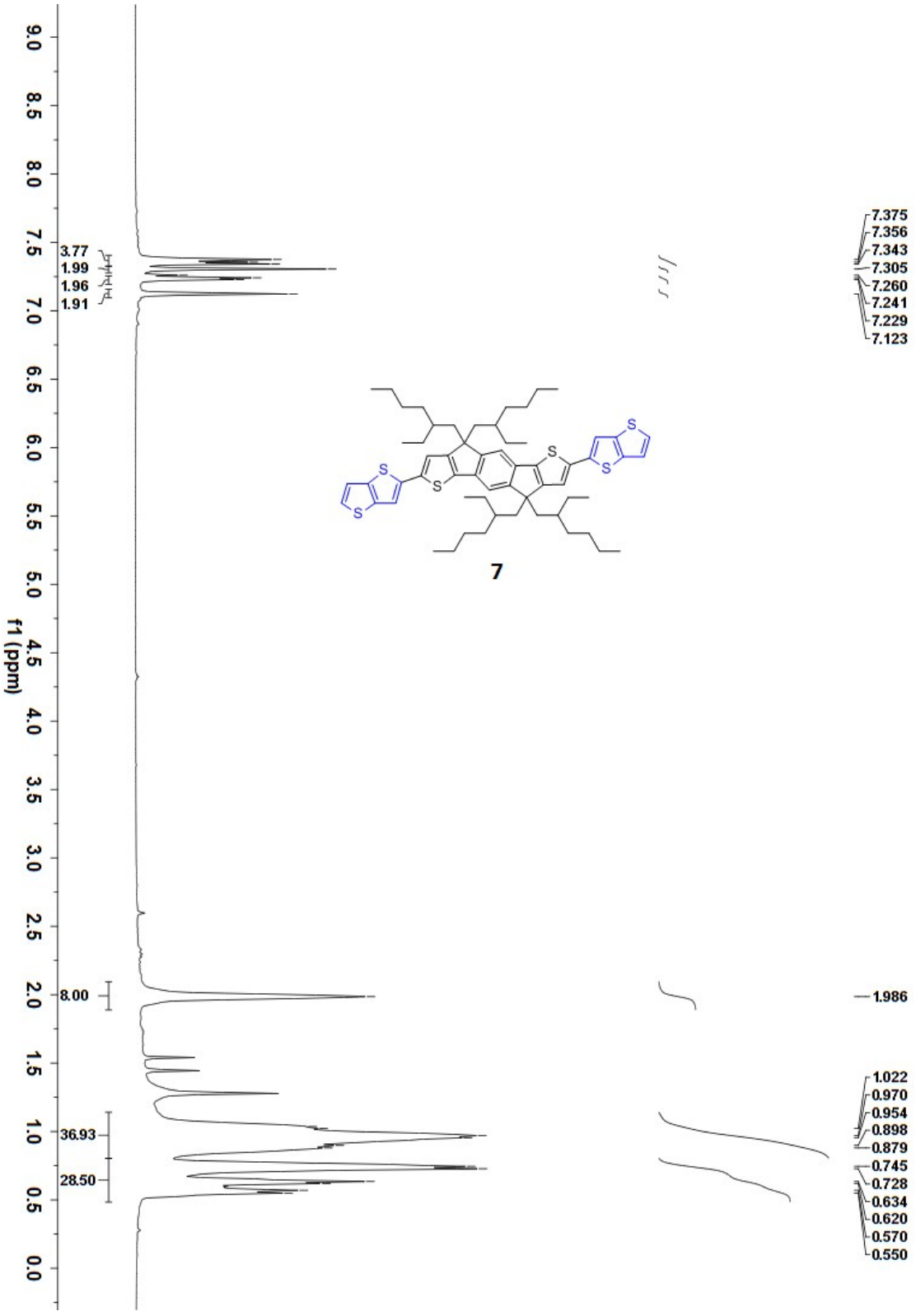

^{1}H NMR spectrum for compound **7**

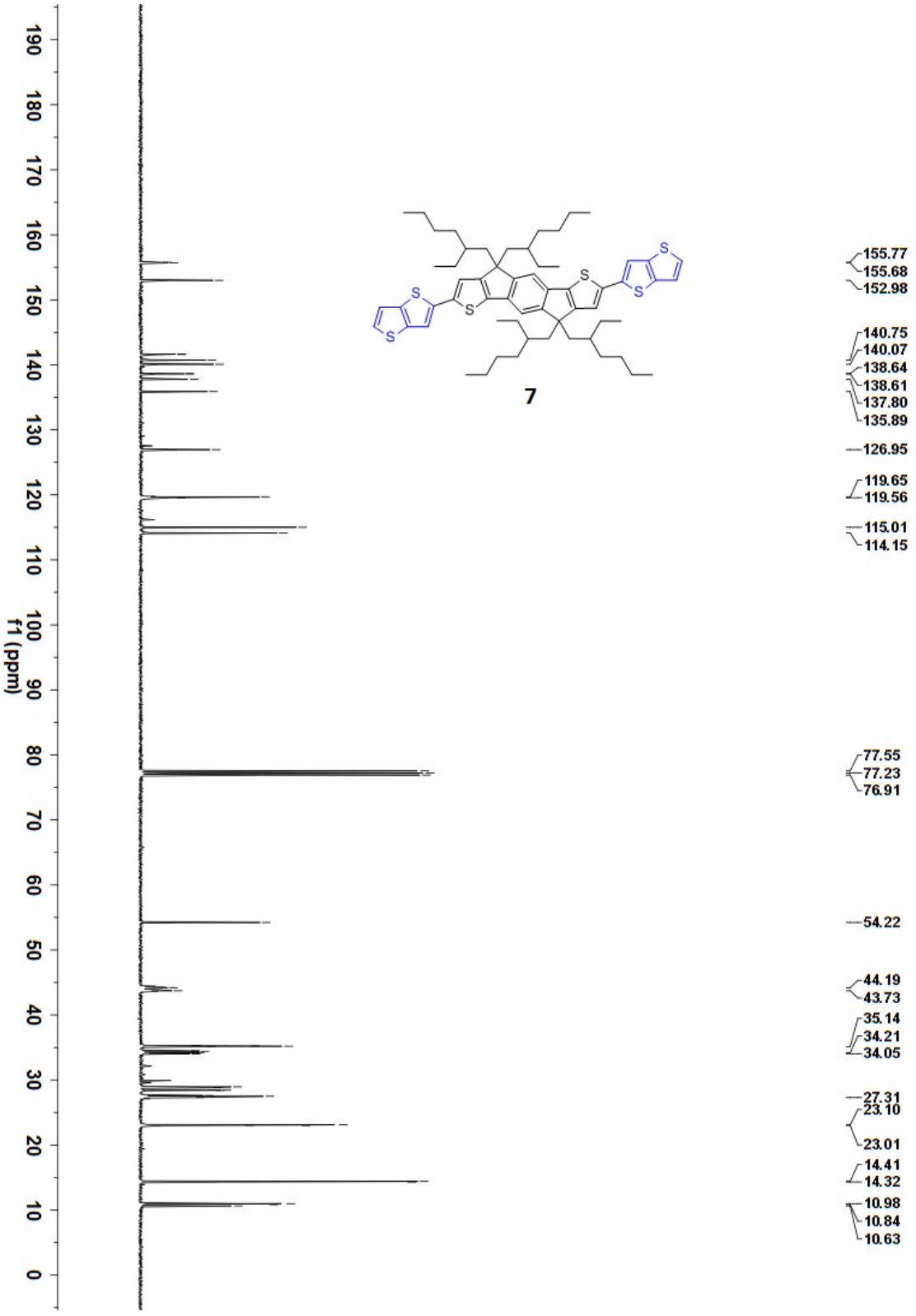

^{13}C NMR spectrum for compound **7**

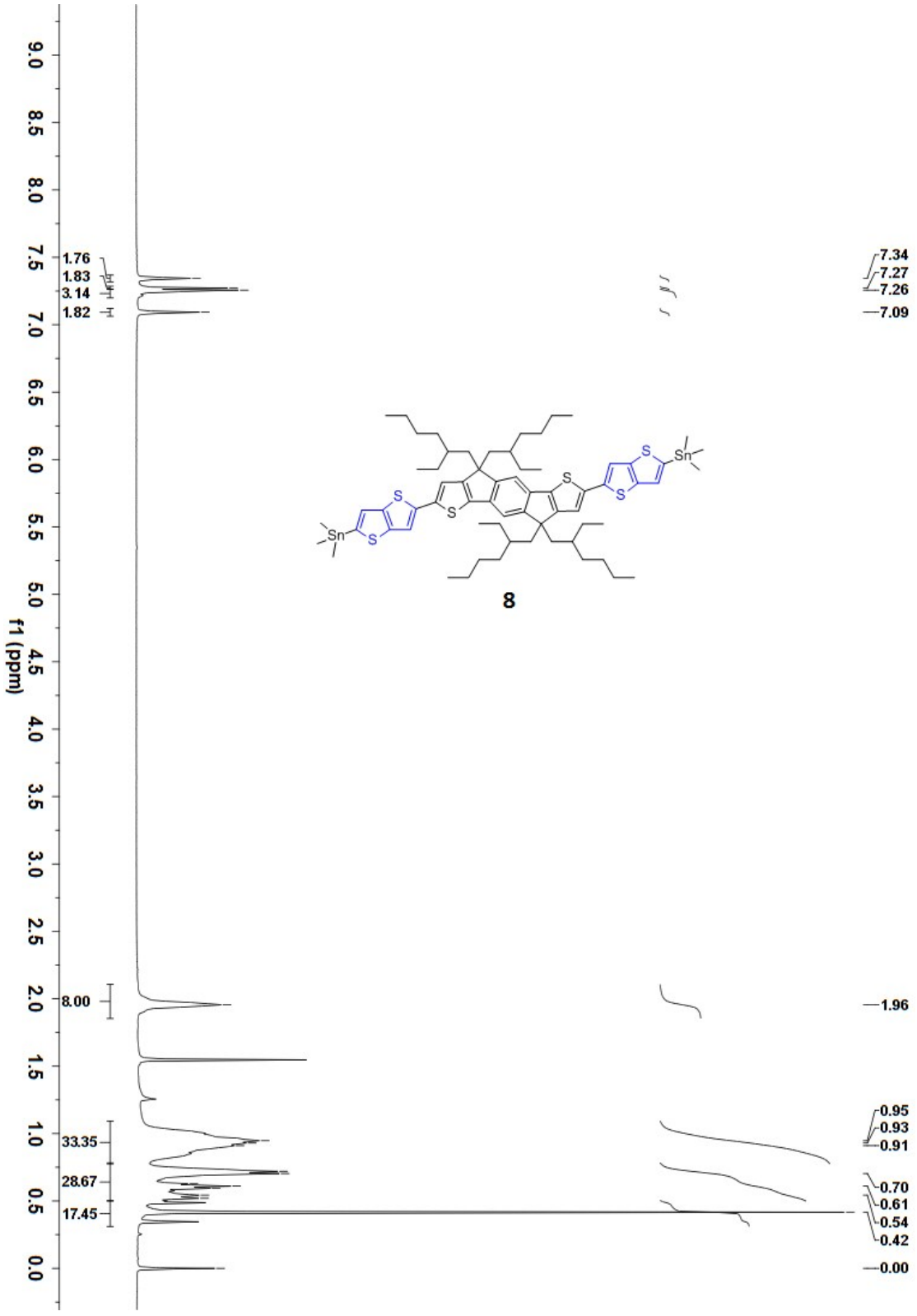

^{1}H NMR spectrum for compound **8**

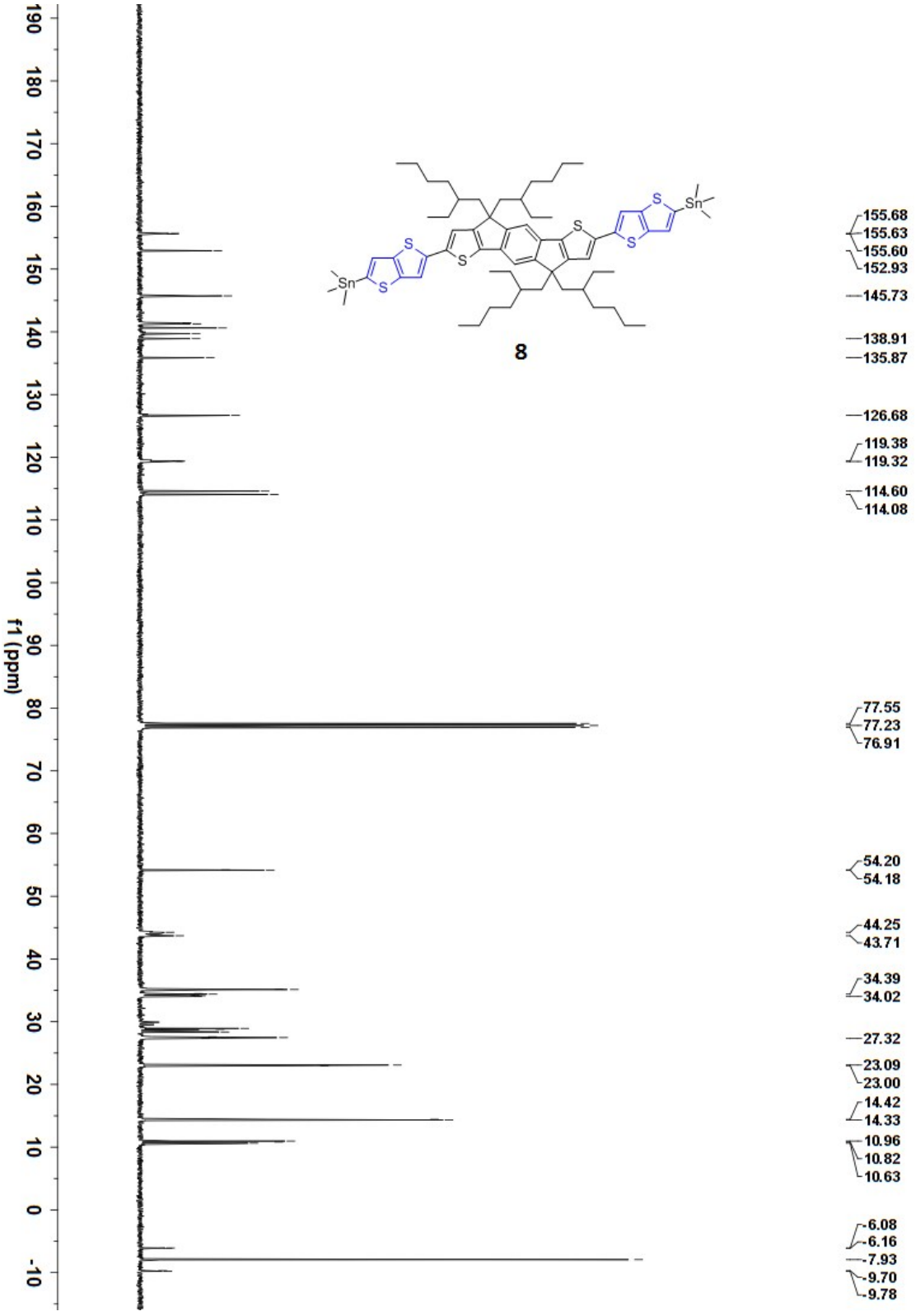

^{13}C NMR spectrum for compound **8**

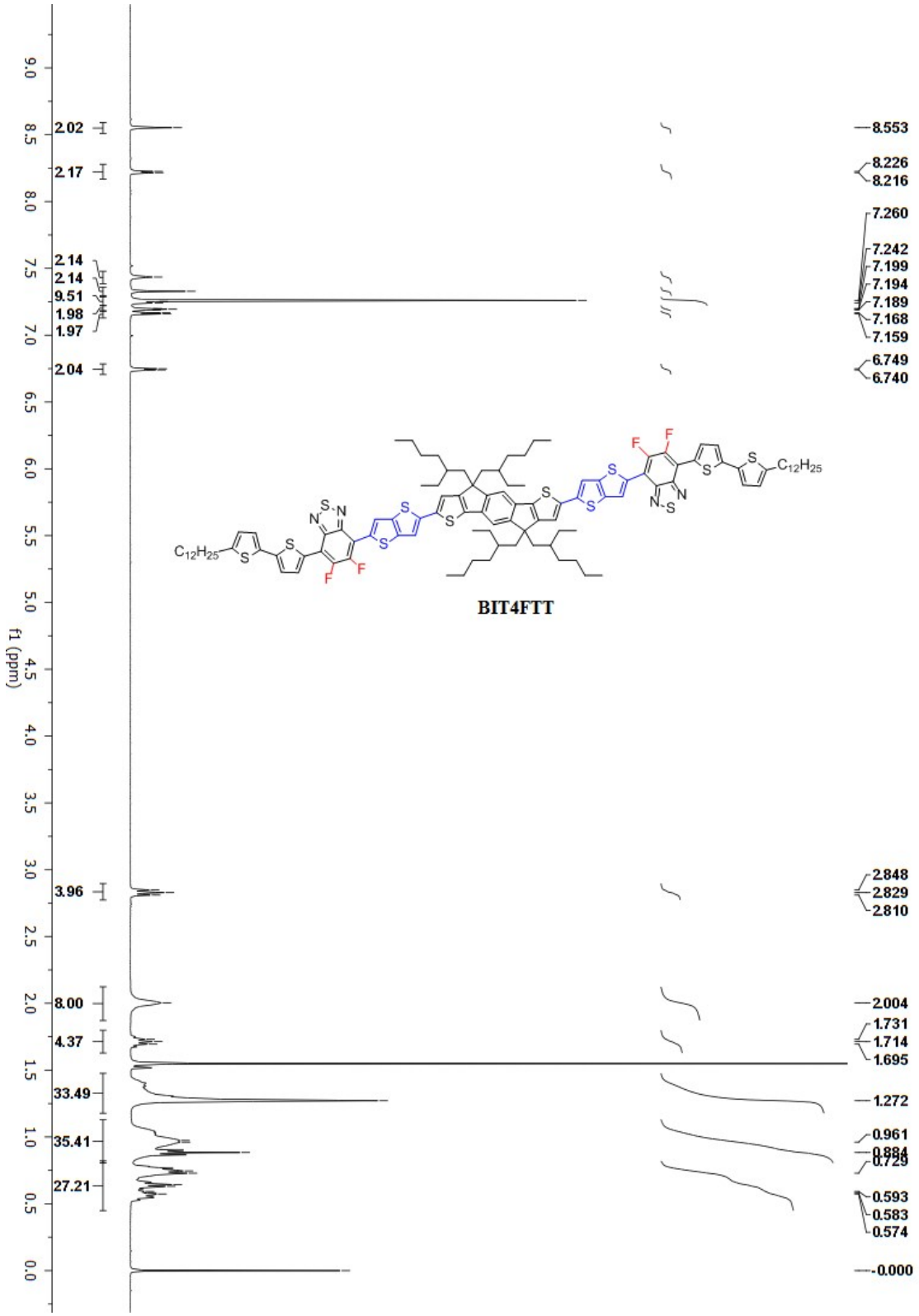

^{1}H NMR spectrum for **BIT4FTT**

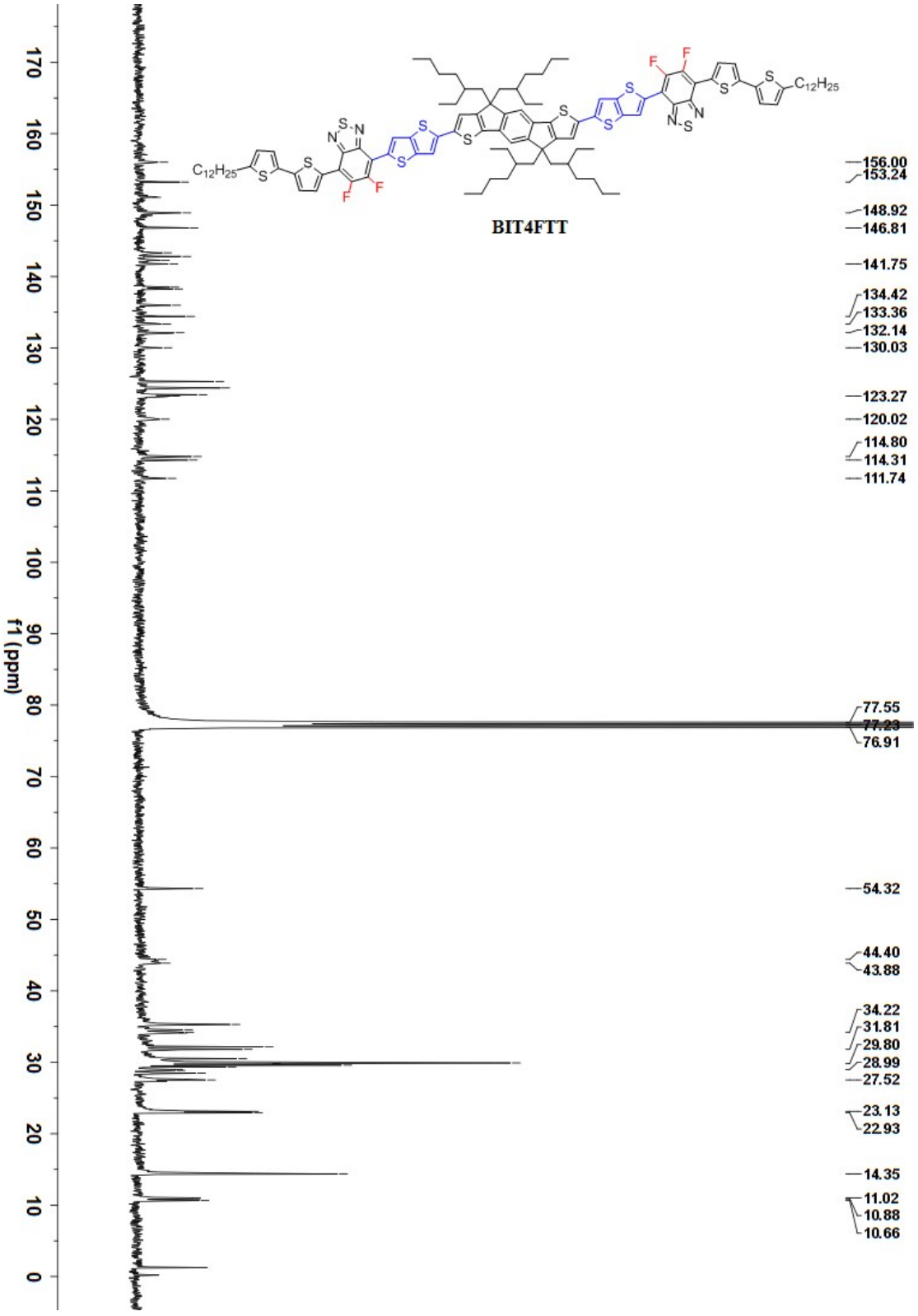

^{13}C NMR spectrum for **BIT4FTT**